https://doi.org/10.5194/essd-2026-65
Preprint. Discussion started: 4 February 2026

Earth System Science Data
Open Access Discussions

TED: A global temperature-driven thermoelastic displacement dataset for GNSS reference stations (2000–2023)

Ran Lu[1,2,3], Zhao Li[1,2], Lingfeng Ye[3], Peng Yuan[4], Yanming Feng[3]

1. GNSS Research Center, Hubei Luojia Laboratory, Wuhan University, No. 129 Luoyu Road, Wuhan 430079, China
2. School of Geodesy and Geomatics, Wuhan University, No. 129 Luoyu Road, Wuhan, 430079, China
3. Faculty of Science, Queensland University of Technology, Brisbane, 4000, Australia
4. GFZ Helmholtz Centre for Geosciences, Potsdam, Germany

Corresponding Author:

* Zhao Li, ✉ zhao.li@whu.edu.cn

Abstract

The nonlinear signals in global GNSS station height time series reflects both non-tidal mass loading (atmospheric, oceanic, and hydrological) and temperature-driven thermoelastic deformation (TED). However, a globally consistent and reproducible TED data product has long been lacking. Here we present a global dataset of vertical TED for ~15,000 GNSS stations spanning 2000–2023, generated using a full-spectrum, layered finite-element model. The model is driven by hourly ERA5 soil-temperature profiles and parameterized with depth-dependent thermophysical properties from the SoilGrids dataset, enabling consistent quantification of TED from semi-diurnal/diurnal variability through seasonal to interannual timescales. Compared with an identical homogeneous-medium benchmark, subsurface stratification typically changes annual amplitudes by ~0.3 mm and shifts the timing of the annual maximum by ~1 month, yielding regionally coherent and smoothly varying spatial patterns. At stations with independent site characterization, the site-constrained solutions agree closely with SoilGrids-based solutions, with annual-amplitude differences of 0.01–0.03 mm and annual-phase differences mostly within 1–3°. Sensitivity tests using ±10% perturbations in thermal expansion, thermal diffusivity, and Young's modulus indicate that annual-cycle amplitude and phase are robust. Globally, annual TED amplitudes are typically 1–2 mm, exceed 2–3 mm at some stations, and reach peak-to-peak values up to ~5 mm, with the largest signals concentrated in arid inland and continental climate regions. When TED corrections are applied together with non-tidal mass-loading corrections, the residual vertical dispersion decreases at most stations, with vertical scatter reduced by up to ~70% at selected sites. The dataset is publicly available for direct use in GNSS coordinate time series correction and related geophysical applications: https://doi.org/10.5281/zenodo.18256342 (Lu et al., 2026).

1. Introduction

Global Navigation Satellite System (GNSS) reference-station coordinate time series provide a fundamental observational basis for quantifying crustal deformation, vertical land

https://doi.org/10.5194/essd-2026-65
Preprint. Discussion started: 4 February 2026

motion, and surface mass redistribution (Clarke et al., 2005; Jiang et al., 2013; Blewitt et al., 2018; Li et al., 2020). In particular, GNSS height records commonly exhibit pronounced annual and semiannual signals together with broadband and nonlinear variability, with amplitudes ranging from several millimetres to about 2 centimetres. A substantial fraction of this variability is non-tectonic, arising from environmental forcing and local site effects, including elastic deformation induced by non-tidal atmospheric, oceanic, and hydrological loading, as well as temperature-driven thermoelastic deformation (van Dam et al., 2007; Fritsche et al., 2012; Fang et al., 2014; Xu et al., 2017; Li et al., 2025). In the absence of consistent, reproducible, and scalable corrections for these contributions, seasonal and nonseasonal motions can bias velocity estimates, inflate apparent noise levels, and obscure subtle geophysical signals, thereby degrading global reference-frame stability and subsequent geophysical interpretation (Altamimi et al., 2023).

Thermoelastic deformation arises from temperature-driven expansion and contraction of the monument and near-surface materials. Temperature perturbations penetrate the ground via heat conduction, generating subsurface thermal strain that is subsequently expressed as elastic displacement (Biot, 1956; Berger, 1975). GNSS observations indicate that shallow thermoelastic effects can explain a substantial portion of the seasonal vertical and horizontal variability in some regions (Romagnoli et al., 2003; Prawirodirdjo et al., 2006). Importantly, the response is not limited to annual timescales: full-spectrum analyses reveal measurable power across a broad frequency range—from semi-diurnal and diurnal bands, through weather-driven variability, to seasonal and interannual fluctuations—with nonseasonal peak-to-peak motions reaching the millimetre level in some areas and therefore detectable by high-precision geodesy (Lei et al., 2020). Thermoelastic deformation can also propagate into global geodetic parameter estimation as a non-loading error source. For example, Wei et al. (2025) reported that thermoelastic effects contribute significantly to the annual variability of the Z component of geocenter motion, implying that improved modelling and mitigation may enhance the consistency of GNSS-based geocenter estimates across independent solutions.

Robust quantification of thermoelastic effects requires temperature forcing that resolves the diurnal cycle, together with broad spatial coverage and a long observational span. When the forcing is represented only by daily means or by a single fixed-UTC sample, diurnal variability is undersampled and can alias into longer periods. Such aliasing can introduce longitude-dependent biases in daily GNSS coordinate solutions and generate spurious low-frequency variability (from seasonal to interannual), thereby compromising cross-regional statistics and hindering robust intercomparisons among correction products (Li et al., 2024). At the same time, publicly available global GNSS coordinate archives now comprise on the order of 15,000 stations, shifting the need for thermoelastic correction from regional case studies toward scalable, operational products. A uniform, reproducible dataset with a clear update pathway is therefore required to enable large-scale processing workflows and objective cross-product evaluation and intercomparison.

Thermoelastic modelling approaches can be broadly categorized into analytical and numerical methods. Analytical formulations commonly rely on half-space assumptions and idealized boundary conditions; they are compact and computationally efficient and are

https://doi.org/10.5194/essd-2026-65
Preprint. Discussion started: 4 February 2026

Open Access Earth System Science Data Discussions

therefore well suited for rapid first-order estimates and process interpretation (Dong et al., 2002; Yan et al., 2009, 2010). A key limitation, however, is that many analytical models assume depth-invariant—or effectively homogeneous—thermophysical properties, which restricts their ability to capture the amplitude and phase shifts introduced by soil–bedrock stratification. Recent work has moved toward more realistic representations. For example, full-spectrum frameworks now incorporate both seasonal and nonseasonal temperature variability together with bedrock depth and type information (Li et al., 2024). Other studies assess how thermoelastic signals contribute to nonlinear components in GNSS heights across different products and processing strategies (Lu et al., 2024). Collectively, these advances indicate that the interpretability and practical utility of thermoelastic signals depend not only on the model class, but also on how subsurface structure is parameterized and how temperature forcing is temporally sampled.

Compared with analytical approaches, finite element methods (FEM) more readily accommodate material heterogeneity and interlayer coupling. They naturally represent the coupled processes of heat conduction and elastic deformation, making them well suited for thermoelastic problems in layered media (Lei et al., 2020). Building on this capability, we implement a full-spectrum layered FEM workflow (FEM_{FL}) at global scale and release a public dataset of temperature-driven vertical thermoelastic displacement (TED) time series for ~15,000 GNSS stations worldwide over 2000–2023 (Lu et al., 2025). The model is driven in the time domain by hourly ERA5 temperature forcing and parameterized with depth-resolved thermophysical properties from the SoilGrids dataset. The release includes quality-control metrics and technical validation. The dataset is designed as a reusable environmental correction that can be applied alongside non-tidal mass-loading products in GNSS processing workflows, supporting more robust vertical land motion estimation, reference-frame stability assessment, and geocenter-related investigations (Altamimi et al., 2023; Wei et al., 2025).

The paper is organized as follows. Section 2 describes the input data, model configuration, and computational workflow. Section 3 presents the main spatiotemporal characteristics of the dataset, provides technical validation, and quantifies its impact on the structure of GNSS vertical residuals. Section 4 documents the data records (file organization, variable definitions, quality flags, and usage guidance) and provides access instructions. Section 5 summarizes applicability and limitations and outlines future updates.

2. Materials and methods

This dataset addresses the need for globally consistent modeling and correction of non-tectonic vertical deformation at continuously operating GNSS stations by providing temperature-driven vertical thermoelastic displacement (TED) time series for ~15,000 stations spanning 2000–2023. The product is generated using a standardized end-to-end workflow (Fig. 1). The workflow harmonizes station selection and temporal coverage, constructs and resamples the temperature forcing, parameterizes vertically layered subsurface properties, runs FEM_{FL} at scale, and performs quality control and consistency checks prior to packaging and release. Station locations and observation spans are compiled from publicly available GNSS station metadata. Near-surface thermal forcing is derived from

https://doi.org/10.5194/essd-2026-65
Preprint. Discussion started: 4 February 2026

ERA5 soil-temperature profiles, and site-specific layered thermo-mechanical properties are constructed from SoilGrids and related global datasets. The resulting vertical thermoelastic response is computed with the FEM_{FL} and distributed in a GNSS-ready, standardized format.

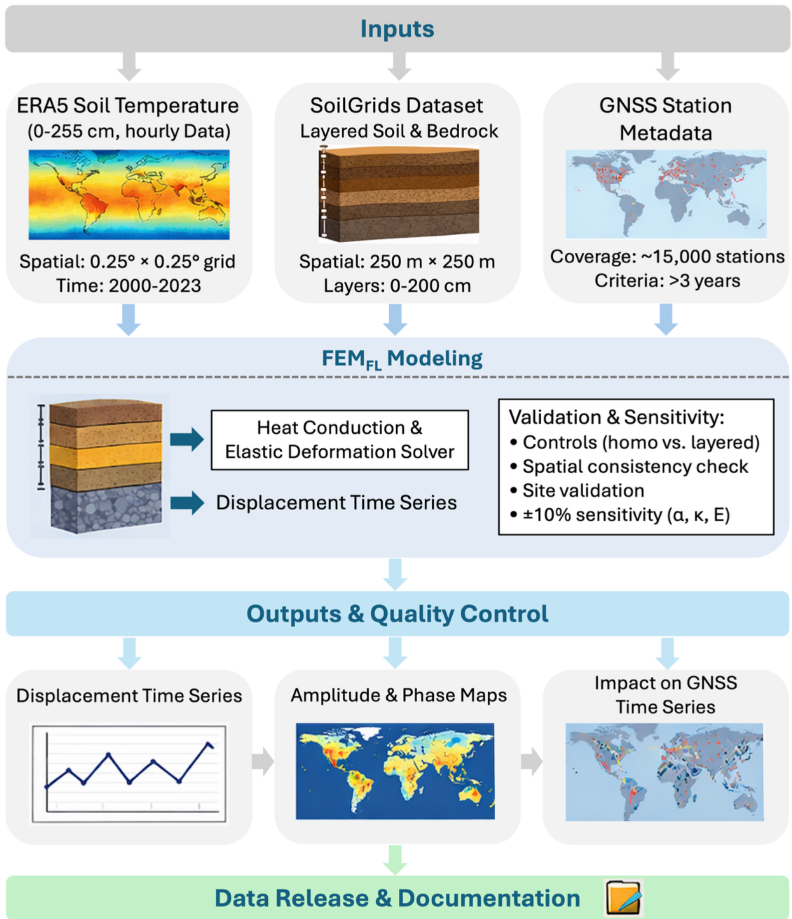

Figure 1 Schematic workflow of dataset production: station selection and metadata compilation; extraction and resampling of ERA5 temperature forcing; retrieval and unified parameterization of layered SoilGrids properties; large-scale FEM_{FL} computation; output quality control and evaluation; and product release (file organization and metadata archiving).

2.1. GNSS station and temporal coverage

GNSS station metadata and coordinate time series are obtained from multi-network solutions compiled and maintained by the Nevada Geodetic Laboratory (NGL), which integrate continuous observations from the International GNSS Service (IGS) and numerous regional and national networks (Blewitt et al., 2018). To support stable estimation of annual and semiannual signals—and to facilitate assessment of potential aliased components

https://doi.org/10.5194/essd-2026-65
Preprint. Discussion started: 4 February 2026

associated with diurnal temperature variability—we retain continuous stations with at least three years of valid observations within 2000–2023, while maximizing the sample size subject to broad global coverage. The resulting dataset includes ~15,000 stations distributed across the major continents and climate zones (Fig. 2), with particularly dense coverage in North America, Europe, East Asia, and Australia. This spatial sampling enables robust regional statistics and provides a basis for internal consistency and quality checks.

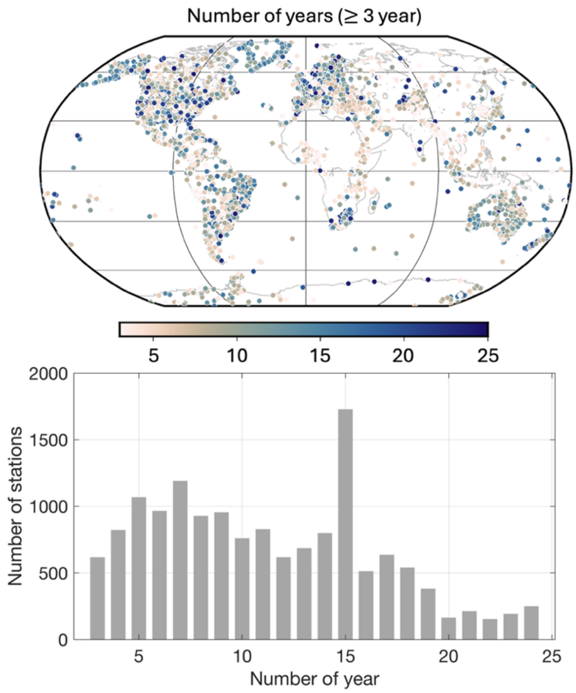

Figure 2 Spatial distribution and temporal coverage of GNSS stations. (a) Global station distribution and available record length (color denotes time-series duration); (b) frequency distribution of available record length.

2.2. Temperature forcing data

The temperature-driven thermoelastic deformation (TED) is induced by near-surface temperature perturbations that propagate downward through heat conduction, generate thermal strain, and are expressed as elastic displacement. The reliability of a TED dataset therefore depends critically on the temporal resolution and phase fidelity of the temperature forcing. We use soil temperatures from ECMWF ERA5 reanalysis as the external forcing and adopt the shallowest layer (soil temperature level 1, 0–7 cm) as a practical proxy for the surface-temperature boundary condition (Hersbach et al., 2018).

To retain sub-daily variability and mitigate the aliasing of diurnal power into lower frequencies associated with fixed-UTC sampling, we sample the hourly ERA5 record at 00, 06, 12, and 18 UTC and apply these values as the upper-boundary forcing at a 6-hour

https://doi.org/10.5194/essd-2026-65
Preprint. Discussion started: 4 February 2026

interval. This strategy maintains global-scale computational tractability while resolving diurnal and semi-diurnal thermal responses. It also reduces spurious seasonal-to-interannual artifacts that can arise when forcing is represented by daily means or by a single-epoch temperature series. In addition to the 0–7 cm layer, we use the full ERA5 soil-temperature profile (0–7, 7–28, 28–100, and 100–255 cm) to better constrain near-surface thermal gradients and to represent background heat transfer at depths.

2.3. Layered thermophysical and mechanical properties

The thermal diffusivity, thermal expansion coefficient, and elastic moduli control how temperature perturbations attenuate and phase-lag with depth and how efficiently thermally induced strain is converted into displacement. Globally consistent TED estimates therefore benefit from site-specific, vertically layered parameterization wherever possible. Here we represent the shallow subsurface using the globally gridded, depth-resolved soil information from SoilGrids (Hengl et al., 2017). SoilGrids provides a suite of soil properties on standard depth intervals (0–5, 5–15, 15–30, 30–60, 60–100, and 100–200 cm), enabling characterization of thermophysical contrasts within the upper ~2 m. We adopted the latest SoilGrids 2.0 dataset that used state-of-the-art machine learning methods to build the required models and produced global maps of soil properties at medium spatial resolution (250 m grid cells) (Poggio et al., 2021).

For each station, we extract the SoilGrids depth profiles and consistently translate them into the thermophysical parameters required by the model (e.g., thermal conductivity or diffusivity and volumetric heat capacity). Mechanical properties (e.g., Poisson's ratio) and the linear thermal expansion coefficient are assigned using a uniform, reproducible lookup table. They are then mapped onto the layered structure, so that spatial variations in soil thickness and shallow properties propagate into the coupled thermo-mechanical response. Below 2 m, where globally consistent high-resolution stratigraphic information is generally unavailable, we represent the deeper medium as a bedrock half-space. Its thermophysical and mechanical properties are prescribed using a unified rule set. This parameterization treatment maintains global computational feasibility and reproducibility while retaining the dominant influence of shallow-layer heterogeneity on the modeled response.

2.4. TED modeling framework

We compute temperature-driven vertical TED using full-spectrum layered finite element model (FEM_{FL}; Lu et al., 2025). Beneath each station, the subsurface is represented as a one-dimensional, vertically layered soil–bedrock column. Layer-specific thermophysical and mechanical properties are derived from SoilGrids and related datasets and are assumed uniform within each layer. The time-varying near-surface temperature is prescribed as the upper boundary condition. Temperature perturbations then propagate downward through transient heat conduction and attenuate with depth, producing depth-dependent thermal strain. Contrasts in thermal diffusivity, linear thermal expansion, and elastic stiffness among layers control both the amplitude damping and phase lag of the temperature field and the efficiency with which thermal strain is converted into elastic deformation. Together these effects produce a measurable vertical displacement at the surface. This unified framework

https://doi.org/10.5194/essd-2026-65
Preprint. Discussion started: 4 February 2026

enforces heat transfer within layers, continuity across interfaces, and thermo-mechanical coupling, enabling consistent and scalable site-specific TED estimates at the global scale.

In the thermal component, the temperature evolution in each layer follows the one-dimensional transient heat-conduction equation. Continuity of temperature and heat flux is imposed at all layer interfaces, ensuring physically consistent energy transfer through the stratified column. The upper boundary temperature is prescribed from the ERA5 soil-temperature forcing, while the lower boundary condition is formulated to represent a stable deep thermal background, thereby limiting nonphysical drift associated with truncating the domain at finite depth. The model is advanced at the same cadence as the forcing (6-hour time steps), retaining variability from sub-daily to seasonal timescales.

In the mechanical component, FEM_{FL} treats temperature-induced thermal strain as an eigenstrain term in the constitutive relation and solves the resulting vertical displacement in a one-dimensional layered finite element system. Within each element, thermal strain is determined by the temperature departure from a reference state and the linear thermal expansion coefficient, whereas elastic moduli govern how this strain translates into displacement and how deformation is transmitted across layer interfaces. Solving the assembled layered column yields the surface-node vertical displacement time series directly, rather than relying on simplified depth-integration approximations, and therefore captures stratification effects on both amplitude and phase more consistently. To suppress start-up transients associated with uncertain deep-temperature initial conditions, we apply a spin-up procedure in which a representative year of temperature forcing is repeated until the deep temperature field converges to a stable annually periodic state. The TED series for 2000–2023 is then generated from this equilibrated initialization.

Daily GNSS coordinate solutions are typically referenced to a fixed UTC epoch, whereas sub-daily temperature forcing—and the resulting thermoelastic response—are phased primarily by local solar time. Using a single UTC sampling time can therefore introduce longitude-dependent artifacts and alias diurnal energy into longer periods. To reduce this sensitivity, we drive FEM_{FL} with temperature forcing sampled at four UTC epochs (00, 06, 12, and 18 UTC). This yields four TED realizations. We then combine them using a phase-consistent strategy. For dominant harmonic components (e.g., annual and semiannual), we apply amplitude–phase vector averaging to preserve both magnitude and phase. The remaining non-harmonic variability is merged on a common sampling basis and added to form the final series. The resulting TED product is less sensitive to the chosen UTC epoch. It is also more compatible with daily GNSS solutions. As a result, it is better suited to large-scale correction workflows.

2.5. Quality control and consistency checks

To facilitate reuse, traceability, and verification, all released time series are subjected to multi-level quality control and consistency checks. First, numerical artefacts are screened, including spikes, step-like discontinuities, and unrealistic long-term drift. For the small subset of stations that fail these checks, likely causes are examined (e.g., gaps or interpolation issues in the temperature forcing, fallback/default parameter assignments, or problems in the layered configuration), and the affected records are either assigned quality

https://doi.org/10.5194/essd-2026-65
Preprint. Discussion started: 4 February 2026

flags or excluded from the release. Second, spectral consistency is assessed by estimating the amplitude and phase of the principal periodic components (semi-diurnal, diurnal, semiannual, and annual), and by verifying that these quantities vary smoothly within comparable climate regimes; this helps limit spurious spatial discontinuities introduced by gridding or parameter transitions. Third, application-oriented checks are performed by applying TED together with non-tidal loading corrections at representative stations and across regional scales, followed by quantifying the resulting changes in GNSS vertical residual statistics (e.g., residual dispersion).

2.6. Model performance metrics

To consistently quantify the key amplitude characteristics of the TED product and its correction impact on GNSS vertical time series, we compute the annual-cycle amplitude and phase, the nonseasonal variability, and the WRMS improvement of GNSS residuals. For each TED series $u(t)$, we fit an annual and semiannual harmonic model with a linear term:

$$u(t) = a_0 + bt + \sum_{k=1}^{2}[c_k cos(\omega_k t) + s_k sin(\omega_k t)] + \varepsilon(t) \tag{1}$$

where a_0 is the constant term, b is the linear term, ω_1 and ω_2 correspond to the annual and semiannual frequencies, respectively, and $\varepsilon(t)$ denotes the residual. The annual amplitude and phase are defined as:

$$A_{ann} = \sqrt{c_1^2 + s_1^2} \tag{2a}$$

$$\phi_{ann} = atan2(s_1, c_1) \tag{2b}$$

To quantify the remaining variability after removing the linear term and the annual/semiannual harmonics, let $\hat{u}(t)$ denote the fitted reconstruction. The residual is $r(t) = u(t) - \hat{u}(t)$, and the nonseasonal variability is measured by the root-mean-square (RMS) of $r(t)$:

$$RMS_{nonsea} = \sqrt{\frac{1}{N}\sum_{i=1}^{N} r(t_i)^2} \tag{3}$$

where N is the number of valid samples.

For the GNSS vertical time series $x(t)$, we quantify scatter using the weighted root-mean-square (WRMS):

$$WRMS = \sqrt{\frac{\sum_{i=1}^{N}\omega_i[x(t_i)-\bar{x}_\omega]^2}{\sum_{i=1}^{N}\omega_i}} \tag{4}$$

$$\bar{x}_\omega = \frac{\sum_{i=1}^{N}\omega_i x(t_i)}{\sum_{i=1}^{N}\omega_i} \tag{5}$$

where the weights are $\omega_i = 1/\sigma_i^2$; when observation uncertainties are unavailable, we use equal weights ($\omega_i = 1$). The WRMS reduction rate is defined as:

$$\Delta WRMS(\%) = \frac{WRMS_{raw} - WRMS_{corr}}{WRMS_{raw}} \times 100\% \tag{6}$$

https://doi.org/10.5194/essd-2026-65
Preprint. Discussion started: 4 February 2026

where $WRMS_{raw}$ and $WRMS_{corr}$ denote the series before and after correction, respectively. We evaluate WRMS improvements for each single correction (NTAL, NTOL, HYDL, and TED) as well as for the combined correction (NTAL+NTOL+HYDL+TED) to quantify the spatially varying contributions of different environmental processes.

In the parameter-sensitivity analysis, we apply a ±10% relative perturbation to a selected key parameter at each station and recompute TED. The difference between the perturbed and baseline solutions in the annual cycle is then quantified as:

$$\Delta A_{ann} = A_{ann}^{(\pm 10\%)} - A_{ann}, \quad \Delta\phi_{ann} = \phi_{ann}^{(\pm 10\%)} - \phi_{ann} \tag{7}$$

where $A_{ann}^{(\pm 10\%)}$ denotes the annual-cycle amplitude after applying a +10% (or −10%) perturbation to the parameter, and $\phi_{ann}^{(\pm 10\%)}$ denotes the corresponding annual-cycle phase. For summary statistics, we use the absolute values $|\Delta A_{ann}|$ and $|\Delta\phi_{ann}|$ to represent the "sensitivity magnitude." For the volcano plots, the empirical significance p_{emp} is defined as the two-sided empirical tail probability within the same (region × parameter) subset:

$$p_{emp} = 2min(F(\Delta), 1 - F(\Delta)) \tag{8}$$

where $F(\Delta)$ is the empirical cumulative distribution function. We plot $-log_{10}(p_{emp})$ as an index of "extremeness" or tail magnitude, emphasizing that it is an empirical measure rather than a hypothesis-test p-value based on a specific statistical assumption.

3. Results and analysis

This section summarizes the spatiotemporal characteristics and practical performance of the global TED time series (2000–2023) generated with FEM_{FL}. We first use representative stations to illustrate TED variability across multiple timescales, and then present global patterns of annual amplitude, annual phase, peak-to-peak range, and nonseasonal variability. Next, regional transects and validation windows are used to evaluate the sensitivity and internal consistency of the layered parameterization. Finally, using GNSS vertical time-series together with residual-dispersion and spectral analyses, we quantify how applying TED in combination with non-tidal mass-loading corrections reduces residual scatter and apparent noise levels. All metrics and their computations are defined in Section 2.6.

3.1. Thermoelastic displacement characteristics

We illustrate typical temperature-driven vertical thermoelastic displacement (TED) behavior using four representative GNSS reference stations—AARS, SHAO, KSCO, and BRO1 (Fig. 3)—selected to span contrasting climatic regimes. At all sites, TED shows a coherent periodic signal with superimposed short-term fluctuations (upper panels). Residuals after removing a linear trend and the annual and semiannual harmonics are shown in the lower panels. Seasonally, TED closely follows the temperature cycle: warm-season expansion

https://doi.org/10.5194/essd-2026-65
Preprint. Discussion started: 4 February 2026

produces uplift, and cold-season contraction produces subsidence. At SHAO, for example, TED typically peaks in July–August and reaches a minimum around January, with an annual amplitude of ~1 mm. Sub-daily variability is also evident, with diurnal fluctuations of ~0.1–0.3 mm that are particularly clear at arid sites with large day–night temperature contrasts (e.g., AARS), highlighting a seasonally dominated signal with detectable sub-daily structure.

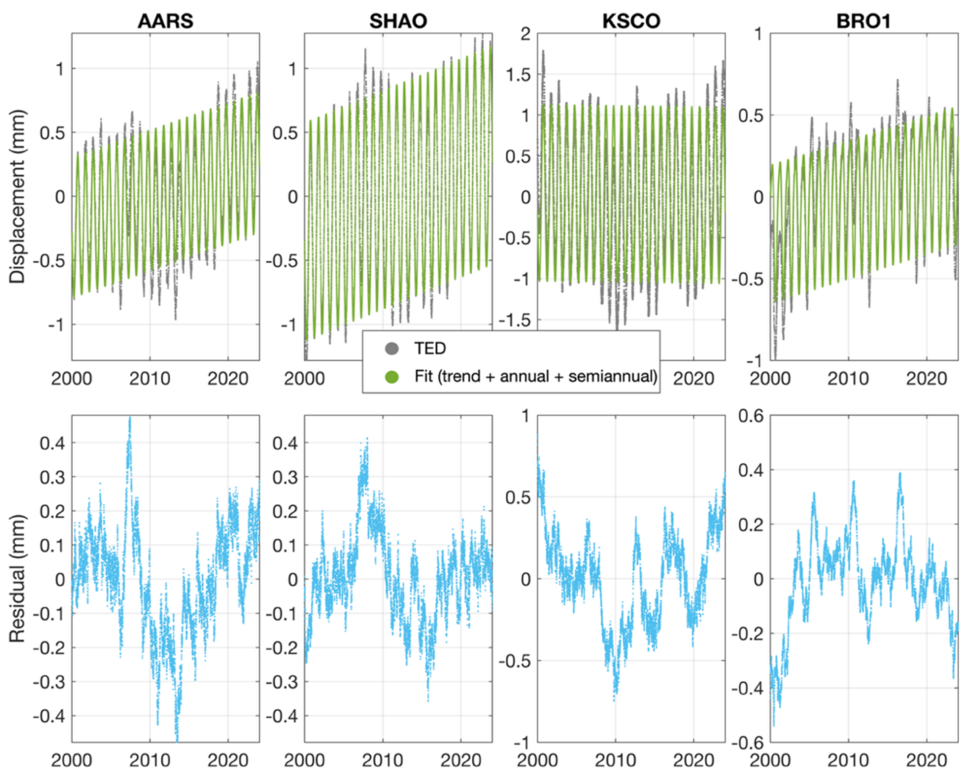

Figure 3 Examples of vertical thermoelastic displacement series at four representative GNSS stations (top: original series with fitted trend plus annual and semiannual harmonics; bottom: residuals after removing trend, annual and semiannual harmonics).

To characterize global TED, we decompose the FEM_{FL} time series at all stations and derive four metrics: annual amplitude and phase, peak-to-peak displacement, and nonseasonal variability. Figure 4 maps the annual amplitude and phase from the homogeneous FEM and layered FEM_{FL} models, along with their differences. Both models display consistent first-order patterns, with larger annual amplitudes over mid–high-latitude continents and continental climates, smaller amplitudes in maritime and humid tropical regions, and pronounced latitudinal structure in annual phase.

Relative to the homogeneous FEM, FEM_{FL} generally yields modestly larger annual amplitudes, most notably in continental interiors. This behavior is physically consistent with layered media: reduced near-surface thermal conductivity and diffusivity steepen shallow

https://doi.org/10.5194/essd-2026-65
Preprint. Discussion started: 4 February 2026

Open Access Earth System Science Data Discussions

temperature gradients and concentrate thermal strain closer to the surface, which amplifies the vertical response. In contrast, effective homogeneous properties tend to smooth this insulating effect. Amplitude differences are predominantly positive, typically ~0–0.3 mm and locally up to ~0.4 mm and are smaller in humid coastal or densely vegetated regions where seasonal temperature forcing is damped. Annual-phase patterns remain broadly similar, but FEM_{FL} introduces measurable shifts in some continental interiors: differences are mostly within ±40° and commonly on the order of a few to a few tens of degrees (e.g., 10°–30°). These shifts are consistent with layering-induced changes in the attenuation and phase lag of downward-propagating temperature variations, and hence in the timing of peak displacement.

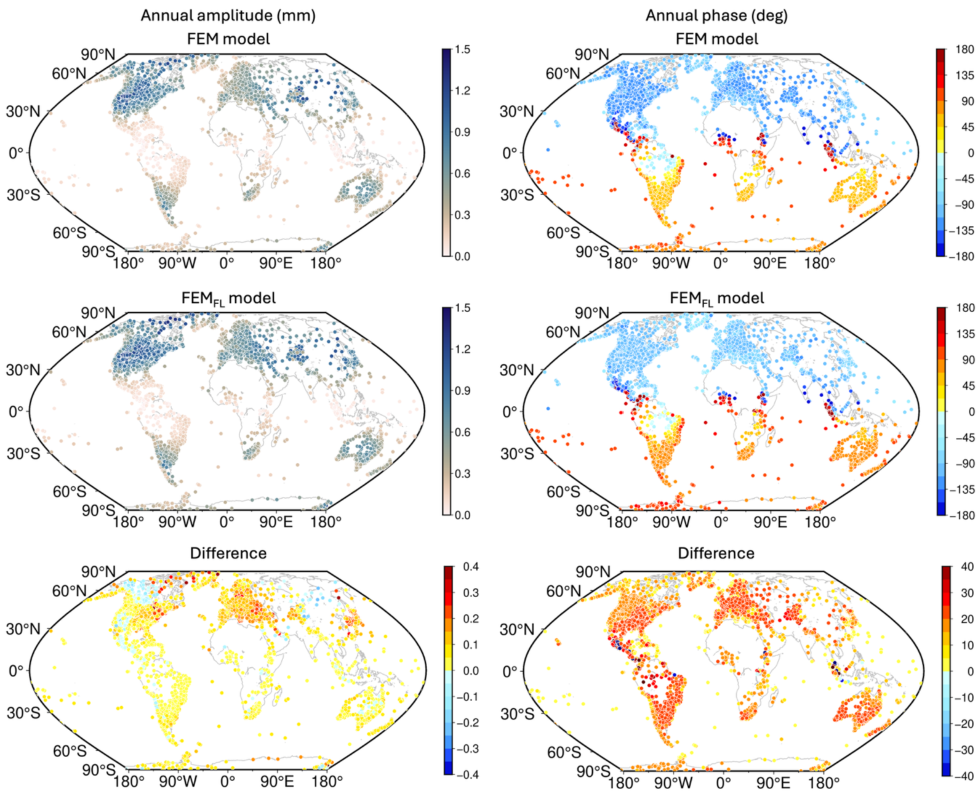

Figure 4 Comparison of annual-cycle amplitude and phase estimated by the homogeneous FEM and FEM_{FL}.

Figure 5 shows global distributions of TED peak-to-peak displacement and nonseasonal variability by comparing results from the homogeneous FEM and layered FEM_{FL} models. Peak-to-peak displacement is defined as the difference between the maximum and minimum TED values over 2000–2023, representing the total range at a site due to the seasonal cycle together with shorter-period fluctuations. The two models show broadly similar spatial patterns, but FEM_{FL} generally yields larger ranges: peak-to-peak values are typically ~2–4 mm and reach ~5 mm at the upper end. The FEM_{FL} minus FEM differences are

https://doi.org/10.5194/essd-2026-65
Preprint. Discussion started: 4 February 2026

predominantly positive, commonly 0–1 mm and locally approaching ~2 mm, indicating that layered parameterization tends to increase the total displacement range, particularly where short-period temperature variability is strong.

Nonseasonal variability is quantified from the residual series after removing a linear trend and the annual and semiannual harmonics, and thus reflects TED variations from diurnal-to-weather timescales as well as interannual to multi-year fluctuations. Relative to the homogeneous FEM, FEM_{FL} produces slightly higher nonseasonal variability overall: the differences are dominated by small positive values, but locally reach contrasts of up to ~±2 mm. This pattern is consistent with reduced near-surface conductivity and diffusivity concentrating temperature perturbations within shallow layers, which amplifies higher-frequency thermoelastic strain and, in turn, increase the residual variance. Figure 5 therefore indicates that subsurface layering influences not only seasonal amplitudes, but also the overall displacement range and nonseasonal variability, with the largest impacts in continental interiors.

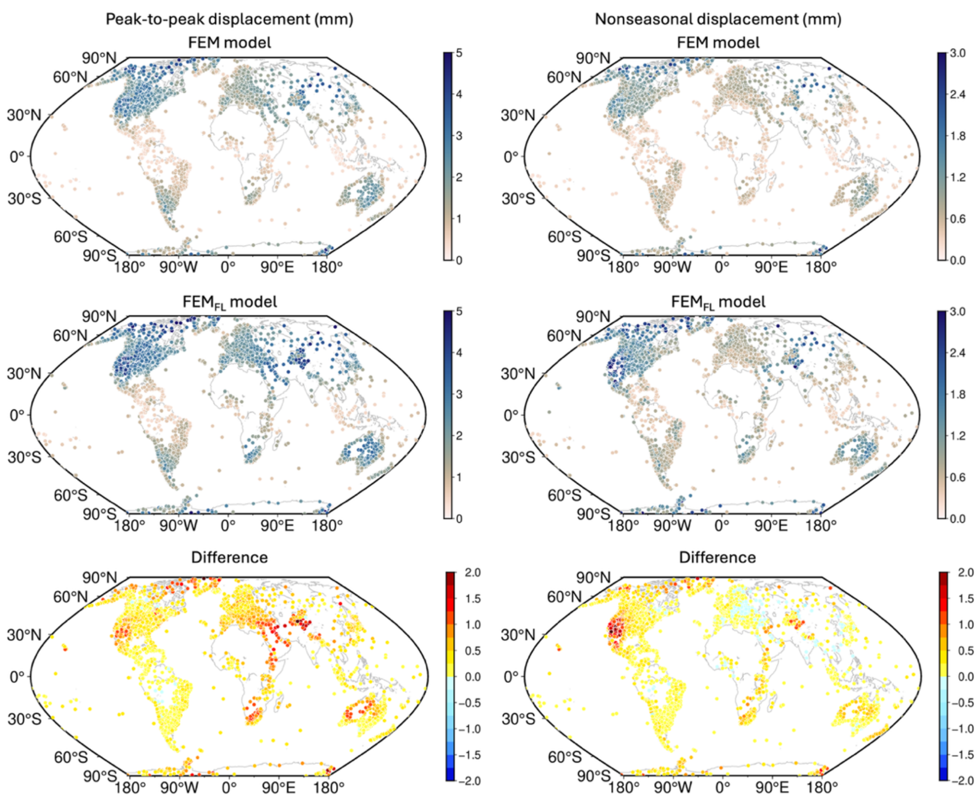

Figure 5 Comparison of peak-to-peak displacement and nonseasonal displacement intensity estimated by the homogeneous FEM and FEM_{FL}.

Figure 6 further summarizes FEM_{FL}-estimated TED peak-to-peak displacement through (i) latitudinal statistics, (ii) regional groupings, and (iii) spectral characteristics. The latitudinal

https://doi.org/10.5194/essd-2026-65
Preprint. Discussion started: 4 February 2026

Open Access Earth System Science Data Discussions

analysis shows a clear, systematic dependence of peak-to-peak displacement on latitude. However, the substantial within-band spread (10th–90th percentile range) indicates that latitude alone does not control TED magnitude. Regional climate regimes and shallow subsurface conditions also matter, particularly soil–bedrock stratification and its thermophysical properties. Regional boxplots highlight these contrasts: North America and East Asia show higher median peak-to-peak values, whereas Southeast Asia and Central America are lower, consistent with differences in temperature forcing and near-surface thermal responsiveness. To characterize the frequency content, we compute and stack TED power spectral densities (PSDs) across stations within latitude bands and regions. The stacked spectra show a dominant peak near 1 cycle per year (cpy; annual), secondary peaks at 2 cpy (semiannual) and higher-integer harmonics, and a smoothly decaying high-frequency tail. These patterns prove that TED represents a broadband thermoelastic response with a strong seasonal component and appreciable nonseasonal variability extending from monthly to weather timescales.

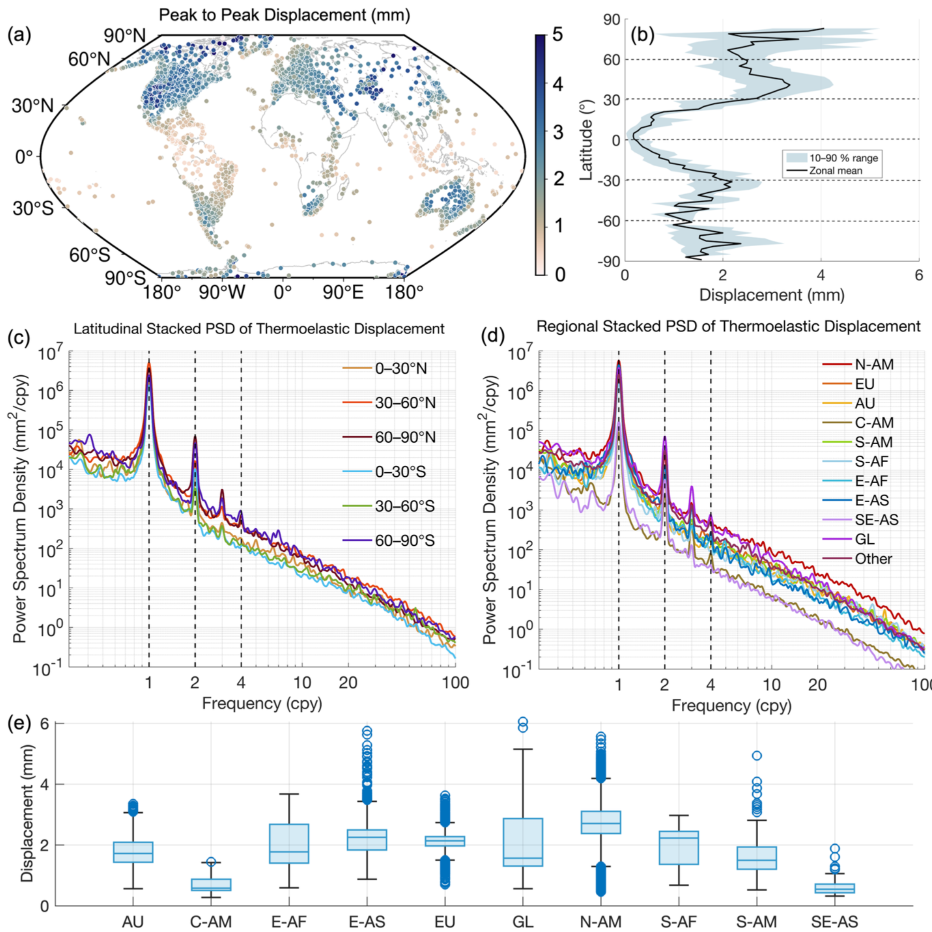

Figure 6 Global distribution, regional statistics, and representative PSD characteristics of

https://doi.org/10.5194/essd-2026-65
Preprint. Discussion started: 4 February 2026

FEM_{FL}-derived TED peak-to-peak displacement. Region abbreviations: N-AM (North America), EU (Europe), AU (Australia), C-AM (Central America), S-AM (South America), S-AF (Southern Africa), E-AF (Eastern Africa), E-AS (East Asia), SE-AS (Southeast Asia), GL (Greenland).

Notably, a weak long-term component is present in TED at some stations. We estimate linear trends for the vertical TED series at each site (Fig. 7) and find that they are generally small, with the vast majority within ±0.2 mm yr^{-1}. However, the trends exhibit coherent spatial structure instead of random scatter. Positive trends dominate globally, whereas negative trends are more localized and may be associated with regional differences in climate and surface conditions, including land cover, soil moisture, and snow or freeze–thaw regimes. Such trend-like behavior may reflect multi-year non-stationarity in the temperature forcing (e.g., regional warming/cooling or long-term drift in reanalysis temperatures) and/or gradual adjustment of the shallow soil–bedrock thermal state toward a shifting multi-year mean. These signals therefore require cautious interpretation and should not be treated as tectonic or other secular geophysical trends. Although small from year to year, these effects can accumulate into millimeter-level offsets over years to decades, biasing long-term vertical velocity estimates and reference-frame stability metrics. We therefore recommend treating the TED trend as a quantifiable temperature-related background term in sensitivity analyses and uncertainty budgets for long-term GNSS velocity and reference-frame applications.

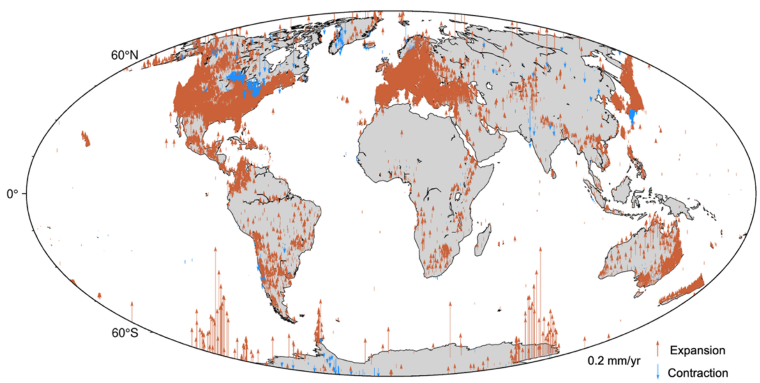

Figure 7 Estimated linear trends of FEM_{FL}-derived thermoelastic displacement time series.

3.2. Reliability assessment of the thermoelastic dataset

To better isolate the influence of subsurface layering on the annual TED signal, we focus on North America as a representative subregion and examine meridional and zonal transects of the SoilGrids-based layered minus the homogeneous solution differences (Fig. 8). These transects summarize how the annual vertical amplitude difference (ΔA) and phase difference (Δϕ) vary with latitude and longitude. The blue curve shows the weighted median after two-dimensional k-nearest-neighbor (2D-kNN) smoothing, the gray envelope denotes the interquartile range (IQR), and the orange tick marks indicate the effective number of stations (N_{eff}) contributing within each smoothing window. Segments with N_{eff} < 5 are

https://doi.org/10.5194/essd-2026-65
Preprint. Discussion started: 4 February 2026

Open Access Earth System Science Data Discussions

plotted as dashed lines and are intended to convey only the broad trend.

The layered model yields slightly larger annual amplitudes than the homogeneous model across most North America locations. The amplitude difference (ΔA) is predominantly positive, typically 0–0.2 mm and reaching ~0.25 mm in a few latitude–longitude segments. This pattern is consistent with shallow thermophysical contrasts strengthening near-surface temperature gradients and concentrating thermoelastic strain toward the surface, thereby modestly enhancing the annual vertical response. Phase differences show greater spatial variability: Δϕ is generally on the order of tens of degrees (about 10–25° across most segments) and forms coherent structures where station density is high. This indicates that subsurface layering affects not only the amplitude but also the timing of the annual maximum, most likely by modifying the effective penetration depth and phase lag of the downward-propagating temperature wave and, in turn, the resulting thermo-mechanical coupling. The differences remain modest overall (ΔA up to ~0.3 mm; Δϕ up to ~30°). Nonetheless, the persistent positive ΔA in continental interiors, together with systematic phase adjustments, is consistent with the expectation that reduced near-surface thermal diffusivity (i.e., stronger insulation) enhances shallow thermoelastic expansion and alters the phase lag.

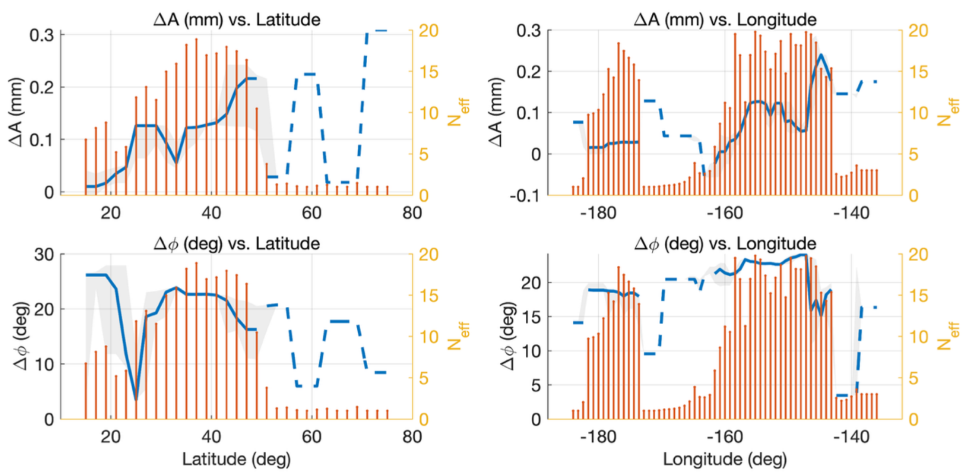

Figure 8 North America case study: meridional and zonal profiles of annual amplitude and phase differences between the SoilGrids-layered solution and the homogeneous solution: $\Delta A = (A_{\text{SoilGrids}} - A_{\text{homo}})$, $\Delta \phi = (\phi_{\text{SoilGrids}} - \phi_{\text{homo}})$. The blue curve shows the 2D-kNN–smoothed weighted median, the gray shading denotes the IQR, and the orange bars indicate N_{eff}; segments with $N_{\text{eff}}<5$ is shown as dashed lines.

To evaluate the robustness of FEM_{FL} across varying site conditions, we select GNSS stations with relatively complete site documentation and perform an independent comparison within four well-instrumented validation windows (Fig. 9). For each station, we construct a site-constrained layered model using available information on

https://doi.org/10.5194/essd-2026-65
Preprint. Discussion started: 4 February 2026

monument/foundation type, embedment depth, and material properties, estimate the annual TED amplitude and phase, and compare these against the SoilGrids-based layered solution. For interpretability, stations are grouped by foundation embedment depth: deep foundations are expected to be more strongly coupled to the stable deeper medium (e.g., bedrock or competent deep soil), whereas shallow foundations are more strongly influenced by near-surface soils. The map in Fig. 9 shows the validation sites and their foundation depths (color-coded), and the boxplots summarize the annual amplitude difference (ΔA) and phase difference (Δϕ) between the site-constrained and SoilGrids-based solutions for the deep and shallow groups in each window (sample sizes in parentheses).

The two parameterizations agree closely. Across the four validation windows, ΔA is on the order of 10^{-2} mm (typically 0.01–0.03 mm) and Δϕ is generally within a few degrees (about 1–3°). This indicates that, where site surveys are unavailable, gridded SoilGrids thermophysical properties provide a reasonable statistical representation of typical conditions and that FEM_{FL} is not unduly sensitive to moderate parameter differences. Shallow-foundation sites show slightly higher medians and larger dispersion in both ΔA and Δϕ, consistent with greater sensitivity to near-surface thermal processes and local material heterogeneity, whereas deep-foundation sites exhibit tighter distributions and more consistent behavior across windows. This independent validation supports the transferability of FEM_{FL} for global application and suggests that incorporating station-specific information, where available, can further refine local estimates of annual amplitude and phase. Since detailed foundation-depth and material metadata remain sparse across global GNSS networks, the small discrepancies observed here also support SoilGrids-based layering as a practical and physically plausible default for global thermoelastic corrections.

https://doi.org/10.5194/essd-2026-65
Preprint. Discussion started: 4 February 2026

Open Access Earth System Science Data Discussions

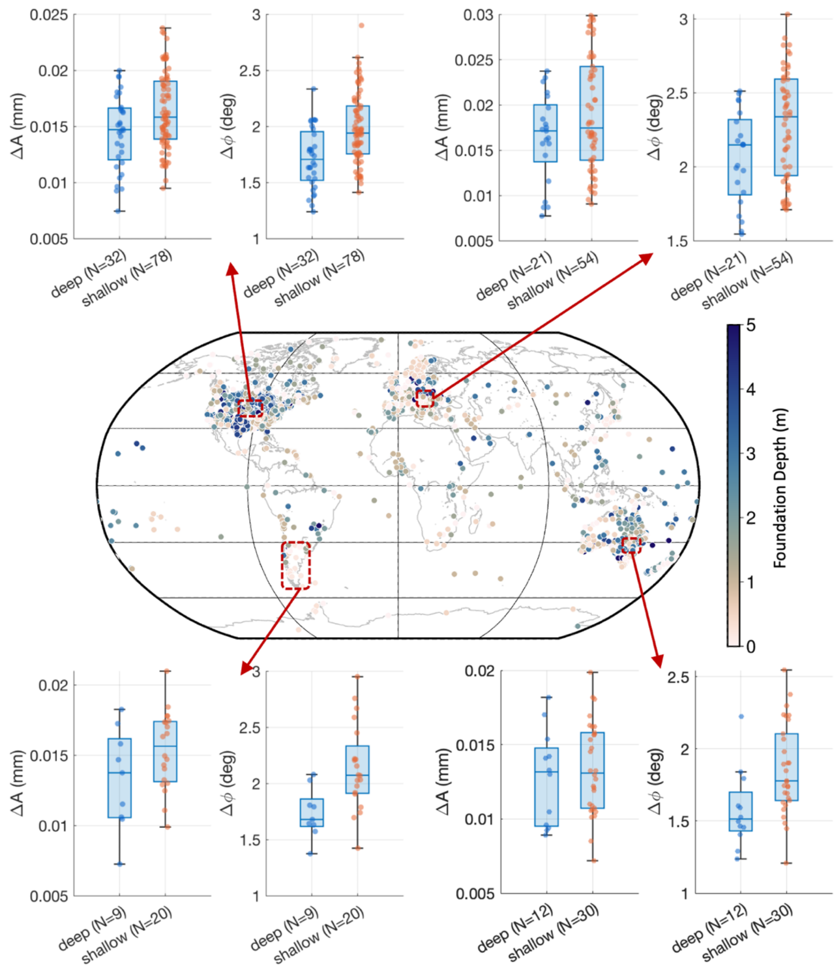

Figure 9 Local validation of FEM_{FL} using stations with known foundation depth and material information: the annual amplitude and phase differences between site-specific layered solution and the SoilGrids-layered solution, shown separately for deep and shallow foundation stations.

Figure 10 summarizes the distribution of absolute changes in annual TED amplitude and phase ($|\Delta A_{ann}|$ and $|\Delta\phi_{ann}|$) induced by ±10% perturbations to key thermo-mechanical parameters, stratified into three representative climate–geographic groups (arid inland, humid coastal, and high-latitude). Across all groups, the responses are concentrated at small values with a limited long tail, indicating that FEM_{FL} is generally robust to moderate parameter uncertainty while allowing for stronger sensitivity at a small subset of stations. The arid-inland group shows the largest dispersion in both $|\Delta A_{ann}|$ and $|\Delta\phi_{ann}|$, consistent with stronger annual temperature forcing and steeper near-surface thermal gradients that can amplify uncertainty in thermal expansion and diffusivity. The humid-coastal group exhibits the tightest distributions (smaller medians and interquartile ranges), reflecting

https://doi.org/10.5194/essd-2026-65
Preprint. Discussion started: 4 February 2026

smoother, ocean-moderated forcing and more stable downward propagation of thermal signals. The high-latitude group is intermediate overall but displays a more pronounced tail at some sites, plausibly linked to snow/freeze–thaw conditions and strong seasonal temperature contrasts. In terms of parameter influence, the linear thermal expansion coefficient α most directly controls $|\Delta A_{ann}|$ (amplitudes scale approximately with α), thermal diffusivity κ primarily affects $|\Delta\phi_{ann}|$ by governing penetration depth and phase lag, and Young's modulus E modulates amplitudes through material stiffness with typically intermediate sensitivity. These patterns provide a basis for uncertainty propagation and help prioritize parameters for further refinement.

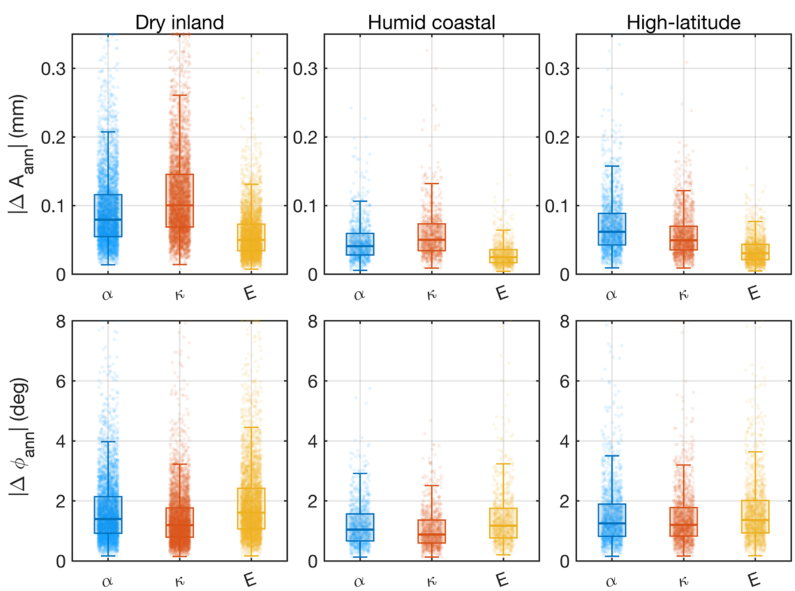

Figure 10 Distribution of TED annual-cycle sensitivity under ±10% parameter perturbations. Box-and-scatter summaries for three region types (arid interior, humid coastal, and high latitude), showing changes in the TED annual cycle when α (linear thermal expansion coefficient), κ (thermal diffusivity), and E (Young's modulus) are perturbed by ±10%.

Figure 11 further quantifies sensitivity using a perturbation-magnitude–empirical-significance framework. The x-axis shows the signed perturbation-induced changes in annual amplitude and phase (ΔA_{ann} and $\Delta\phi_{ann}$), and the y-axis plots $-\log_{10}(p_{emp})$, where p_{emp} is the within-group empirical tail probability and measures how atypical a station's response is for a given (region, parameter) combination. The resulting volcano plots exhibit a characteristic V-shape: most stations cluster near zero change (large p_{emp}; low significance), whereas a small subset shows larger responses (small p_{emp}; high significance) and therefore appears higher on the y-axis. This representation captures both response magnitude and relative rarity, separating pervasive low-level variability from a limited number of genuinely sensitive sites. It enables efficient global identification of station

https://doi.org/10.5194/essd-2026-65
Preprint. Discussion started: 4 February 2026

classes and regions that merit closer scrutiny (e.g., arid-inland and some high-latitude environments) and supports rapid screening using threshold lines. The volcano plots are consistent with boxplot summaries, indicating that annual TED estimates are generally robust to moderate parameter uncertainty while exhibiting interpretable high-sensitivity tails under specific environmental conditions, motivating the use of sensitivity flags or screening rules in quality control and downstream applications.

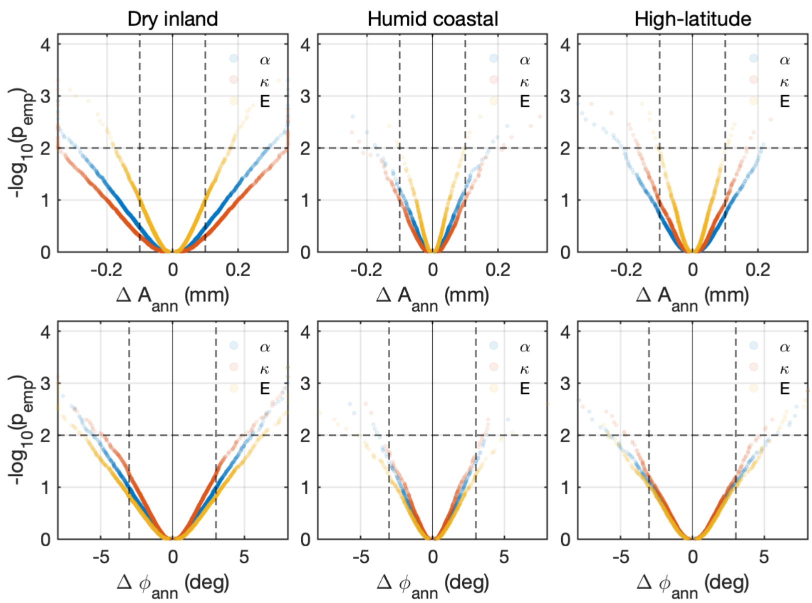

Figure 11 Volcano plots of TED annual-cycle sensitivity: ΔA_{ann} and $\Delta\phi_{ann}$ induced by ±10% parameter perturbations and their empirical significance (p_{emp}).

3.3. Contribution of thermoelastic effects to GNSS motion

To illustrate how temperature-driven TED and non-tidal mass-loading corrections affect GNSS vertical time series, we show examples for four representative stations (AARS, SHAO, KSCO, and BRO1; Fig. 12). For each station, the upper panel displays the four environmental displacement components (NTAL, NTOL, HYDL, and TED), highlighting their relative contributions across seasonal and subseasonal timescales. The lower panel compares the original GNSS vertical series with the corrected residual obtained after removing the combined signal (NTAL+NTOL+HYDL+TED). Before correction, all stations exhibit pronounced seasonal variability along with varying levels of nonseasonal fluctuations; after correction, both the residual dispersion and the seasonal peak-to-trough range are substantially reduced, indicating that these processes account for a large fraction of the non-tectonic vertical signal. At SHAO, for example, the strong annual cycle in the raw series is largely suppressed after correction, leaving mainly small-amplitude higher-frequency

https://doi.org/10.5194/essd-2026-65
Preprint. Discussion started: 4 February 2026

variability and slowly varying residual structure. The dominant contributors vary by site: HYDL is often larger in monsoon-influenced regions, TED tends to be more prominent in arid or continental climates, and coastal stations show an additional NTOL contribution.

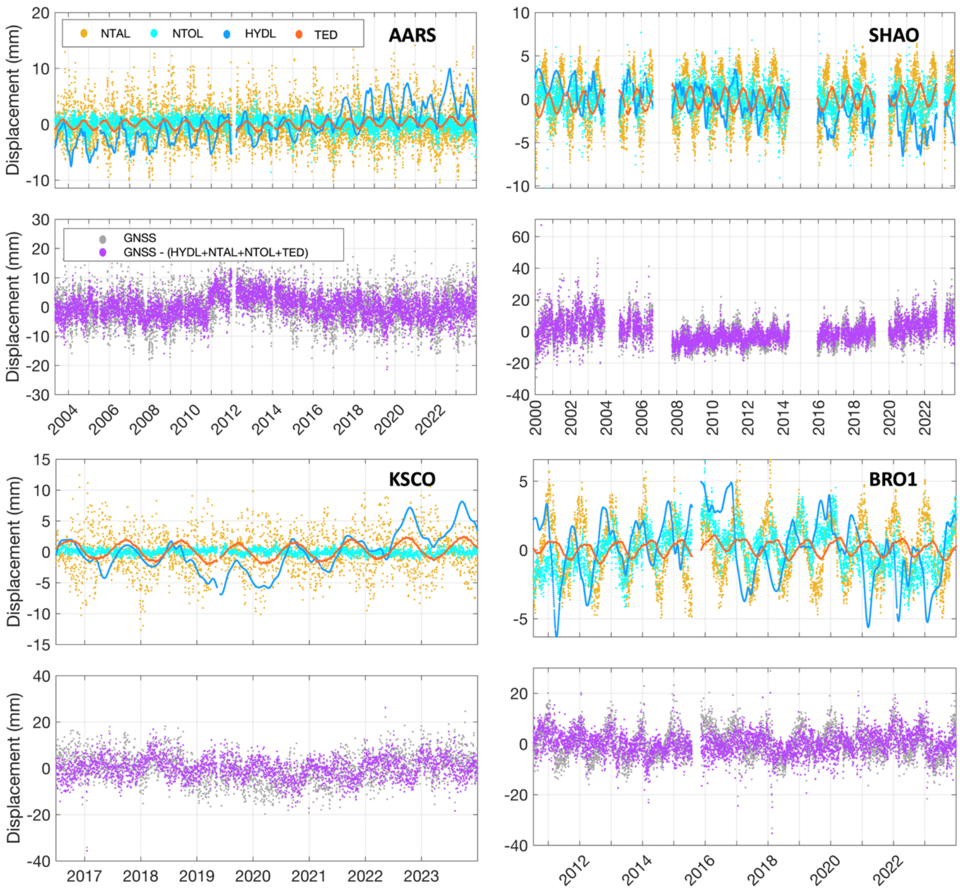

Figure 12 Component comparison and correction effect at four representative stations: the top panels show modeled displacements from NTAL, NTOL, HYDL, and TED, and the bottom panels compare the raw GNSS vertical series with the corrected series after removing these components.

To compare the frequency-domain contributions of TED and non-tidal mass loading to vertical variability of GNSS stations, we compute power spectral densities (PSDs) for four representative stations (Fig. 13). We show PSDs for the raw GNSS height series, the modeled components (FEM_{FL}-TED, HYDL, NTOL, and NTAL), and the temperature forcing (right axis). The GNSS spectra displays a dominant peak near 1 cpy (annual), with secondary peaks near 2 cpy (semiannual) at some sites, together with elevated power at lower frequencies, indicating the coexistence of seasonal and longer-period variability. The temperature forcing concentrates power near 1 cpy, and TED exhibits a co-located annual peak, indicating that

https://doi.org/10.5194/essd-2026-65
Preprint. Discussion started: 4 February 2026

the surface-temperature cycle is efficiently expressed as thermoelastic motion. HYDL and NTAL (and NTOL at coastal sites) also contribute appreciable power in the same seasonal bands, implying that the observed GNSS seasonal peaks typically reflect superposition of multiple environmental processes. Figure 13 is limited to ≤100 cpy and therefore does not include diurnal and semi-diurnal frequencies (≥365 cpy). For daily solutions, sub-daily thermoelastic variability is more likely to influence this band through aliasing rather than as resolvable spectral peaks. The PSD comparison thus provides complementary evidence that both TED and non-tidal loading contribute substantially to GNSS vertical power at the key seasonal frequencies.

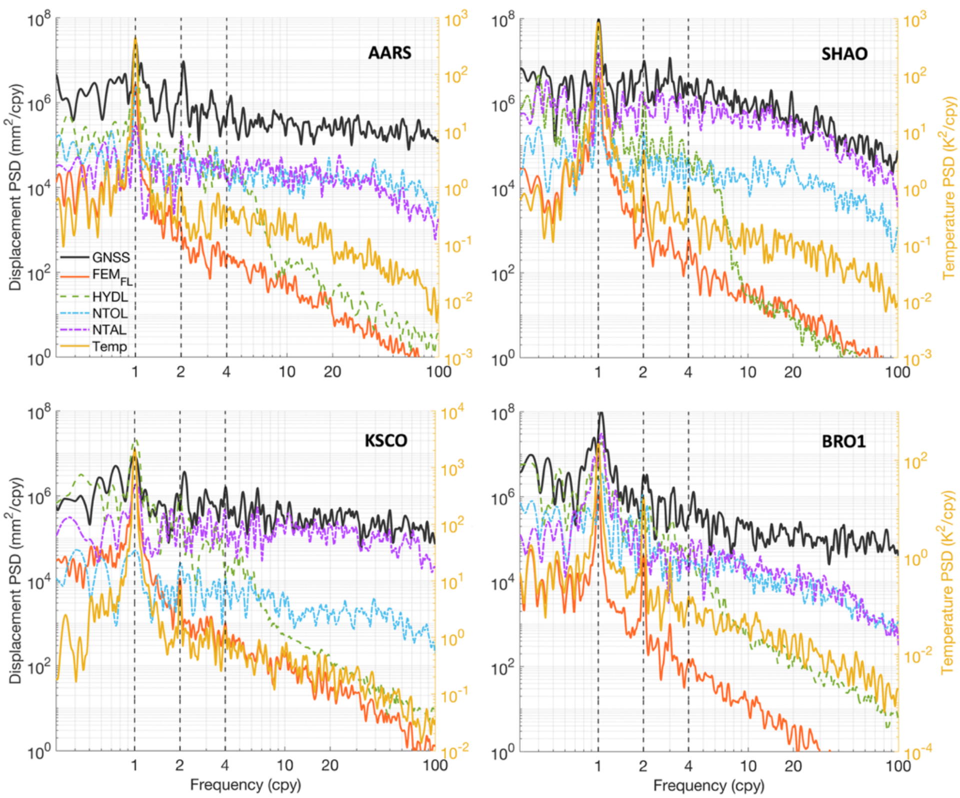

Figure 13 Power spectral density (PSD) comparison for representative GNSS stations: vertical GNSS displacement versus modeled components, including FEM_{FL} thermoelastic displacement, HYDL, NTOL, NTAL, and the temperature-forcing spectrum.

To quantify the contribution of individual environmental processes to GNSS vertical scatter, we apply four corrections separately at each station—NTAL, NTOL, HYDL, and TED—using an identical processing and evaluation scheme. The benefit of each single correction is quantified as the percentage change in the weighted root-mean-square (WRMS) residual dispersion relative to the uncorrected series. Figure 14 summarizes these changes using global maps and regional boxplots for each component. The correction effectiveness is

https://doi.org/10.5194/essd-2026-65
Preprint. Discussion started: 4 February 2026

strongly region dependent and broadly reflects the underlying forcing. HYDL yields the largest reductions in regions with strong seasonal water-storage variability (e.g., monsoon regions, the Amazon basin, and snow-affected high latitudes), where residual dispersion commonly decreases by ~10–30% and locally by ~30–40%. NTAL shows a more spatially extensive impact, with larger improvements in mid–high latitudes and some high-elevation areas, typically reducing dispersion by a few percent to >10%. NTOL primarily affects coastal and island stations and is weak inland, but can still reduce dispersion by a few percent and locally by up to ~10% near coasts with strong seasonal sea-level variability or complex geometry. TED provides a more ubiquitous but generally modest benefit: dispersion reductions are typically a few percent (often ~5%) and are more pronounced in continental arid/semi-arid interiors with large diurnal temperature ranges. For each component, a small subset of stations shows increased dispersion after correction, indicating limited benefit or slight degradation where local effects dominate, noise levels are high, or the correction is not well matched to site conditions. These results underscore that atmospheric, oceanic, hydrological, and thermoelastic effects dominate in different regions, and that no single correction can substitute for the others at global scale.

When the major environmental corrections—NTAL, NTOL, HYDL, and TED—are applied jointly, a larger fraction of the seasonal and low-frequency non-tectonic variability in GNSS vertical time series is explained, resulting in a substantial reduction in residual scatter. Figure 15 maps the resulting percentage reduction in WRMS residual dispersion relative to the uncorrected series, with regional zoom-ins for North America, Europe, Asia, South America, Africa, and Australia. Relative to the single-component corrections (Fig. 14), the combined correction produces a more spatially continuous and regionally coherent improvement. WRMS reductions exceed 10% at most stations and are largest where multiple environmental signals are pronounced and station coverage is dense (e.g., North America, Europe, and parts of East Asia), typically reaching 20–35% and peaking at ~70% in the best cases. This pattern indicates that vertical scatter in these regions is largely driven by the superposition of atmospheric, hydrological, oceanic, and temperature-related effects acting within overlapping frequency bands. Improvements are generally smaller in humid tropical regions, some islands, and sparsely instrumented areas, and a small subset of stations shows near-zero or negative changes, consistent with limited benefit where local nonlinear processes, site effects, or observational noise dominate. Applying TED along with non-tidal loading thus provides an effective global strategy for suppressing major non-tectonic signals, reducing residual noise and low-frequency scatter, and yielding cleaner time series for reference-frame stability assessment, vertical land motion studies, and detection of subtler geophysical signals.

https://doi.org/10.5194/essd-2026-65
Preprint. Discussion started: 4 February 2026

Open Access Earth System Science Data Discussions

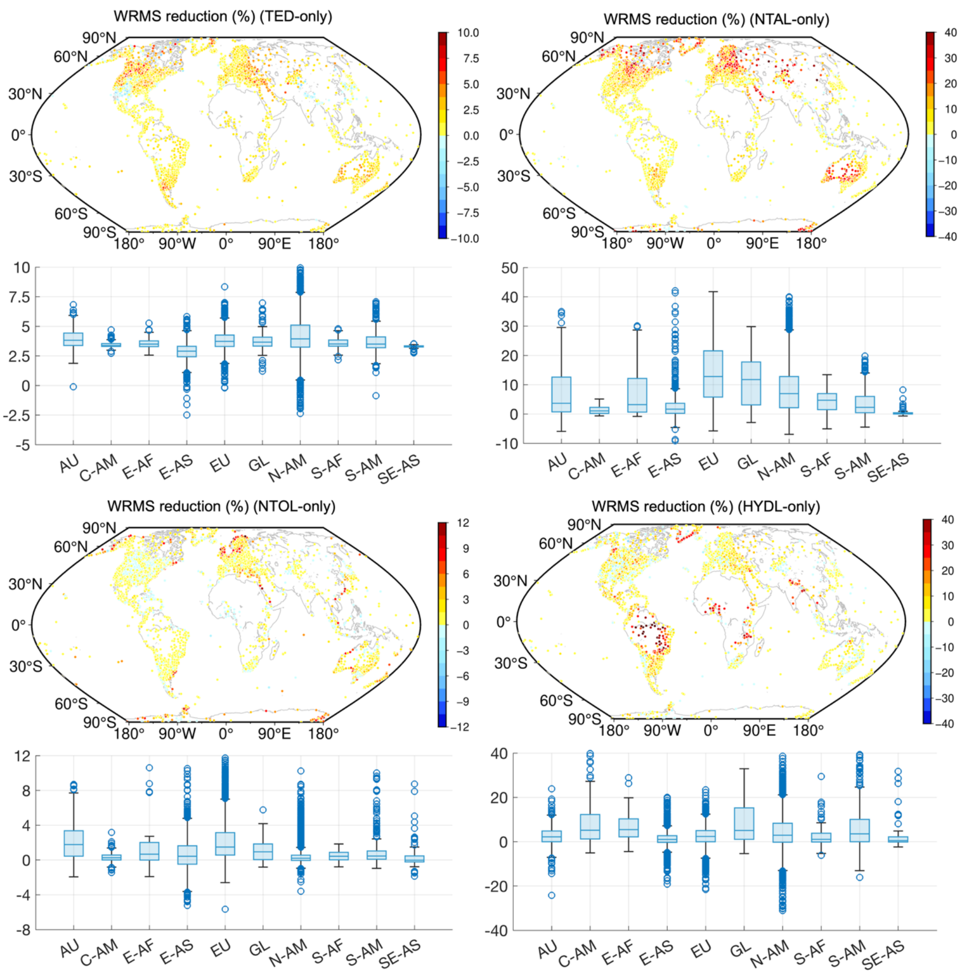

Figure 14 Percentage reduction in WRMS after applying NTAL, HYDL, NTOL, and TED corrections individually, shown as global maps and regional boxplots. Regional abbreviations are consistent with those in Fig. 6e.

https://doi.org/10.5194/essd-2026-65
Preprint. Discussion started: 4 February 2026

Open Access Earth System Science Data Discussions

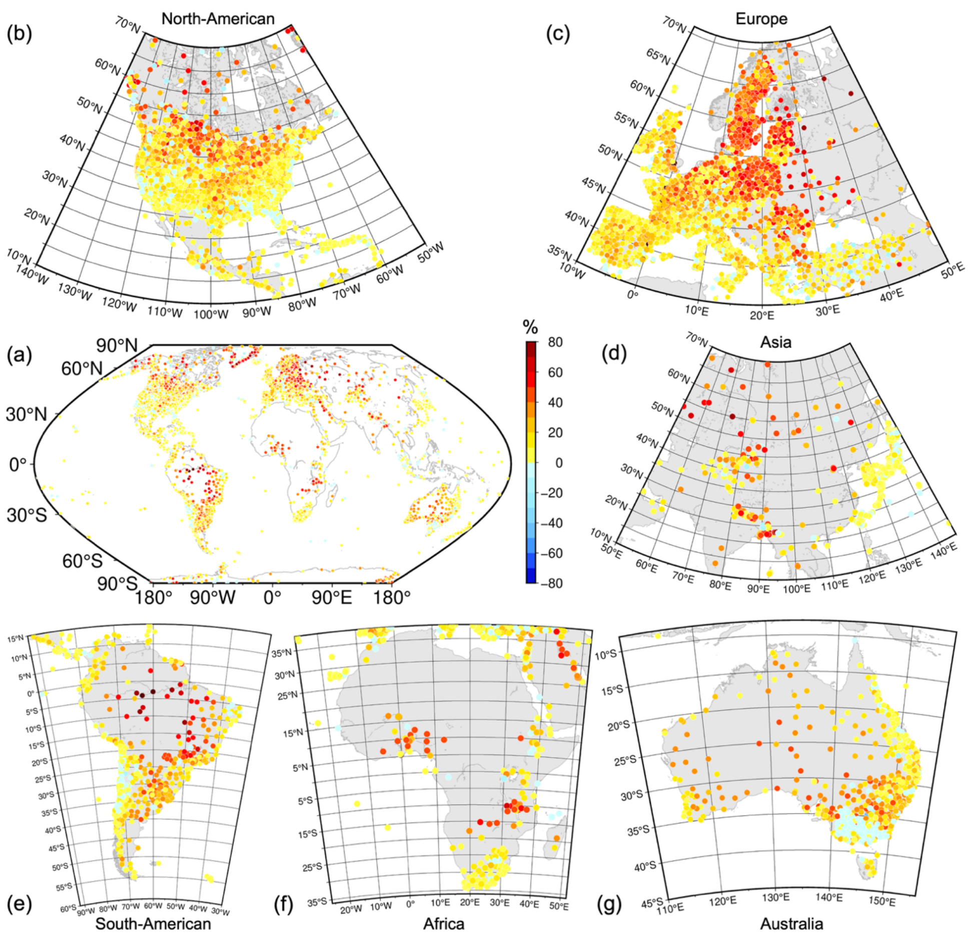

Figure 15 Vertical WRMS reduction after jointly applying NTAL, HYDL, NTOL, and TED corrections: global map and regional zoom-ins.

4. Data availability

The global dataset of temperature-driven vertical thermoelastic displacement (TED) time series for continuous GNSS stations was produced following the workflow described in Section 2 and covers ~15,000 stations for 2000–2023. The archived release is available via Zenodo (DOI: 10.5281/zenodo.18256342; Lu et al., 2026) and is mirrored on the Ground Motion Data Service (GMDS) platform, where users can query by station name and time span and download station-level TED time series together with associated metadata. Data files are organized by station and provide time tags (UTC) and vertical TED displacements (mm), along with essential metadata (e.g., station latitude/longitude, record start/end dates, dataset version, and quality flags), enabling direct alignment with GNSS height time series for correction and evaluation workflows. Users should cite the Zenodo DOI and, when

https://doi.org/10.5194/essd-2026-65
Preprint. Discussion started: 4 February 2026

Open Access Earth System Science Data Discussions

accessing data through GMDS, also cite the GMDS landing page together with the dataset version (if applicable) and the access date.

5. Conclusion and discussion

Correction-ready, multi-decade non-tectonic displacement time series are essential for GNSS reference-frame stability assessments and long-term, wide-area deformation analyses. However, strong heterogeneity in site conditions, temperature forcing, and temporal sampling has hindered a globally consistent and reproducible characterisation of temperature-driven thermoelastic deformation. To address this gap, hourly ERA5 soil-temperature forcing is combined with depth-resolved thermophysical properties from SoilGrids, and a full-spectrum layered finite-element model is implemented globally, producing a global dataset of vertical thermoelastic displacement (TED) time series for ~15,000 continuous GNSS stations over 2000–2023, released openly via the GMDS platform. Methodologically, the dataset couples layered thermo-mechanical physics with a broadband response spanning semi-diurnal/diurnal through seasonal and interannual timescales. To mitigate diurnal aliasing and longitude-dependent artefacts associated with fixed-epoch sampling in daily GNSS solutions, the model is evaluated at four UTC epochs (00/06/12/18) and the four UTC-epoch realizations are combined using a phase-consistent scheme. This strategy retains sub-daily variability while reducing undersampling- and aliasing-related artefacts, yielding daily TED series that align directly with standard daily GNSS height products for practical correction.

Results reveal pronounced regional contrasts in TED. Peak-to-peak displacements are typically at the millimeter level, generally larger in arid interiors and continental climates, but smaller in maritime environments and persistently humid regions. Relative to a homogeneous-medium assumption, incorporating subsurface layering produces systematic increases in annual amplitude and shifts in the timing of the annual maximum in some areas, indicating that site-specific parameterization of depth-dependent thermophysical properties is important for globally consistent TED estimates. Independent validation using 256 stations with site documentation across four well-instrumented regions shows that the SoilGrids-based layered solution agrees closely with site-constrained layered models, with annual-amplitude differences typically 0.01–0.03 mm and annual-phase differences generally within ~1–3° (with a slightly larger spread at shallow-foundation sites). In practical applications, applying TED together with non-tidal loading corrections (NTAL/NTOL/HYDL) reduces seasonal—and part of the nonseasonal—variability in GNSS vertical time series at most stations and produces broadly consistent decreases in residual dispersion, typically 20–35% in densely instrumented regions (e.g., North America, Europe, and parts of East Asia), reaching ~70% at the best-performing sites. Collectively, these improvements support more robust tectonic-velocity estimation, cleaner separation of non-tectonic signals, and millimeter-level reference-frame establishment.

Nevertheless, several limitations remain. First, because the dataset relies on globally uniform inputs, we adopt the simplifying assumption that the monument foundation is tightly coupled to the surface and shallow subsurface, and we cannot yet incorporate station-specific engineering information (e.g., foundation type, embedment depth, and

https://doi.org/10.5194/essd-2026-65
Preprint. Discussion started: 4 February 2026

materials) in a systematic way. As a result, the obtained TED amplitude and phase may be biased for rooftop installations, deep-anchored monuments, or other atypical configurations. Users are therefore encouraged to consult site logs or independent metadata to filter stations, stratify analyses, or perform sensitivity tests to mitigate structure-related biases. Second, SoilGrids provides static thermophysical properties, and we do not explicitly represent processes such as time-varying soil moisture, freeze–thaw phase change, or pore-water migration that can modulate effective thermal diffusivity and phase lag. These omissions may increase uncertainty in seasonally frozen or permafrost regions and in strongly monsoonal humid climates. Future work could integrate permafrost, soil-moisture, and snow datasets to develop seasonally varying effective-parameter schemes, thereby improving model fidelity in complex environments. Third, the temperature forcing is derived from reanalysis, and regional biases or surface energy-balance errors may project into weak low-frequency components over multi-year periods. We therefore treat the TED linear term primarily as a diagnostic quantity rather than a tectonic indicator, and recommend consistent detrending in long-term velocity analyses and, where possible, cross-validation against independent temperature or surface energy-flux observations.

Author contributions

RL proposed the initial idea, designed the experiments, developed the software, and wrote the manuscript. ZL and YF reviewed and revised the manuscript, focusing on the paper structure, correctness of concept, data, and analysis. LY assisted in developing the GMDS website. PY reviewed and revised the manuscript. All authors approved of the manuscript.

Competing interests

The contact author has declared that none of the authors has any competing interests.

Disclaimer

Publisher's note: Copernicus Publications remains neutral with regard to jurisdictional claims made in the text, published maps, institutional affiliations, or any other geographical representation in this paper. While Copernicus Publications makes every effort to include appropriate place names, the final responsibility lies with the authors.

Acknowledgments

We gratefully acknowledge the Nevada Geodetic Laboratory (NGL) for providing the GNSS coordinate time series, GFZ for the non-tidal atmospheric and ocean loading displacement products (NTAL and NTOL), and the GRACE/GRACE-FO Mascon solutions provided by NASA that were used to derive the hydrological loading (HYDL). We also thank ECMWF for the ERA5 temperature datasets. Figures were generated using the Generic Mapping Tools (GMT) software (Wessel et al., 2013). Ran Lu thanks the China Scholarship Council (CSC) for supporting the portion of this work carried out at the Queensland University of Technology (QUT), Australia.

https://doi.org/10.5194/essd-2026-65
Preprint. Discussion started: 4 February 2026

Financial support

This research was supported in part by the National Natural Science Foundation of China (grant nos: 424B2026, 42574041, 42192531, 42388102) and by the Scientific Research Innovation Capability Support Project for Young Faculty (grant no: SRICSPYF-ZY2025007), and by the Wuhan Natural Science Foundation (grant no: 2024040701010029).

References

Altamimi Z, Rebischung P, Collilieux X, Métivier L, Chanard K (2023). ITRF2020: an augmented reference frame refining the modeling of nonlinear station motions. Journal of Geodesy, 97.

Biot MA (1956) Thermoelasticity and irreversible thermodynamics. Journal of Applied Physics, 27:240–253.

Berger J (1975) A note on thermoelastic strains and tilts. Journal of Geophysical Research, 80(2), 274– 277. https://doi.org/10.1029/JB080i002p00274

Blewitt G, Hammond W, Kreemer C (2018) Harnessing the GPS Data Explosion for Interdisciplinary Science. Eos, 99. https://doi.org/10.1029/2018eo104623

Clarke PJ, Lavallée DA, Blewitt G, van Dam TM, Wahr JM (2005) Effect of gravitational consistency and mass conservation on seasonal surface mass loading models. Geophysical Research Letters 32(L08306).

Dong D, Fang P, Bock Y, Cheng M. K, Miyazaki S. I (2002) Anatomy of apparent seasonal variations from GPS-derived site position time series. Journal of Geophysical Research, 107(B4), ETG-9. https://doi.org/10.1029/2001JB000573

Fritsche M, Döll P, Dietrich R (2012) Global-scale validation of model-based load deformation of the Earth's crust from continental watermass and atmospheric pressure variations using GPS. Journal of Geodynamics, 59–60(1):133–142. https://doi.org/10.1016/j.jog.2011.04.001

Fang M, Dong D, Hager H (2014) Displacements due to surface temperature variation on a uniform elastic sphere with its centre of mass stationary. Geophysical Journal International, 196:194–203. https://doi.org/10.1093/gji/ggt335

Hersbach H, Bell B, Berrisford P, Biavati G, Horányi A, Muñoz-Sabater J, Nicolas J, Peubey C, Radu R, Rozum I, Schepers D, Simmons A, Soci C, Dee D, Thépaut JN (2018). ERA5 hourly data on single levels from 1940 to present [Dataset]. Copernicus Climate Change Service (C3S) Climate Data Store (CDS).

Hengl T, de Jesus JM, Heuvelink GBM, Ruiperez Gonzalez, M, Kilibarda M, Blagotić A, Shangguan W, Wadoux A, Ribeiro E, Kempen B, Leenaars J, Walsh MG, Gonzalez MR (2017). SoilGrids250m: Global gridded soil information based on Machine Learning. PLoS ONE, 12(2), e0169748.

Jiang W, Li Z, van Dam T, Ding W (2013) Comparative analysis of different mass loads methods and their impacts on the GPS height time series. Journal of Geodesy, 87(7), 687– 703. https://doi.org/10.1007/s00190-013-0642-3

https://doi.org/10.5194/essd-2026-65
Preprint. Discussion started: 4 February 2026

Lei J, Chen W, Li Z, Li F, Zhang S (2020) A full-spectrum bedrock thermal expansion model and its impact on the global positioning system height time series. Geophysical Research Letters, 47(1). https://doi.org/10.1029/2019GL086022

Li Z, Chen W, van Dam Tonie, Rebischung Paul, Altamimi Zuheir (2020) Comparative analysis of different atmospheric surface pressure models and their impacts on daily ITRF2014 GNSS residual time series. Journal of Geodesy, 94(4), 1-20. https://doi.org/10.1007/s00190-020-01370-y

Li Z, Lu R, Jiang W, Dong D, Lei J, Lu Y, Ding X, Yang C, Chen H, Chen Q (2024) A refined full-spectrum temperature-induced subsurface thermal expansion model and its contribution to the vertical displacement of global GNSS reference stations. Journal of Geodesy, 98, 25. https://doi.org/10.1007/s00190-024-01834-5

Li Z, Jiang W, van Dam T, Zou X, Chen Q, Chen H (2025) A Review on Modeling Environmental Loading Effects and Their Contributions to Nonlinear Variations of Global Navigation Satellite System Coordinate Time Series. Engineering, 47, 26-37. https://doi.org/10.1016/j.eng.2024.09.001

Lu R, Li Z, Chen Q, Ding X, Yang C, Zhang M, Lu Y, Fan W, Chen H, Jiang W (2024) On the contributions of refined thermal expansion model to nonlinear variations in different GNSS height time series products. GPS Solutions, 28, 80. https://doi.org/10.1007/s10291-024-01625-7

Lu R, Li Z, Ye L, Wang J, Yuan P, Ding X, Zhang M, Feng Y (2025) Diurnal temperature forcing and subsurface stratification drive thermoelastic displacements at global GNSS stations, Journal of Geophysical Research: Solid Earth (Under Review)

Lu, R., Li, Z., Feng, Y. (2026). TED: A global temperature-driven thermoelastic displacement dataset for GNSS reference stations (2000–2023) [Data set]. Zenodo. https://doi.org/10.5281/zenodo.18256342

Romagnoli C, Zerbini S, Lago L, Richter B, Simon D, Domenichini F, Elmi C, Ghirotti M (2003) Influence of soil consolidation and thermal expansion effects on height and gravity variations. Journal of Geodynamics, 35(4-5), 521-539. https://doi.org/10.1016/S0264-3707(03)00012-7

Prawirodirdjo L, Ben-Zion Y, Bock Y (2006) Observation and modeling of thermoelastic strain in southern California integrated GPS network daily position time series. Journal of Geophysical Research, 111, B02408. https://doi.org/10.1029/2005JB003716

Poggio L, de Sousa L M, Batjes N H, Heuvelink G B M, Kempen B, Ribeiro E, Rossiter D (2021) SoilGrids 2.0: producing soil information for the globe with quantified spatial uncertainty, SOIL, 7, 217–240, https://doi.org/10.5194/soil-7-217-2021.

van Dam T, Wahr J, Lavallée D (2007) A comparison of annual vertical crustal displacements from GPS and Gravity Recovery and Climate Experiment (GRACE) over Europe. Journal of Geophysical Research: Solid Earth, 112(B3).

Wessel P, Smith WHF, Scharroo R, Luis J, Wobbe F (2013) Generic mapping tools: improved version released. Eos Trans AGU 94(45):409–410.

https://doi.org/10.5194/essd-2026-65
Preprint. Discussion started: 4 February 2026

Wei N, Zhou Y, Shi C, Xu X, Rebischung P, Liu J (2025) Toward a refined estimation of geocenter motion from GNSS displacements: Mitigating thermoelastic deformation and systematic errors. Journal of Geophysical Research: Solid Earth, 130(7), e2024JB028967.

Xu X, Dong D, Fang M, Zhou Y, Wei N, Zhou F (2017) Contributions of thermoelastic deformation to seasonal variations in GPS station position. GPS Solutions, 21(3), 1265–1274. https://doi.org/10.1007/s10291-017-0609-6

Yan H, Chen W, Zhu Y, Zhang W, Zhong M (2009) Contributions of thermal expansion of monuments and nearby bedrock to observed GPS height changes. Geophysical Research Letters, 36. https://doi.org/10.1029/2009GL038152

Yan H, Chen W, Shu Y, Zhang W, Zhong M, Liu G (2010) Thermal effects on vertical displacement of GPS stations in China. Chinese Journal of Geophysics (in Chinese), 53(4): 825-832.